Kinetics and Free Energy Gaps of Electron-Transfer Reactions in *Rhodobacter sphaeroides* Reaction Centers†

V. Nagarajan,*,‡ W. W. Parson,‡ D. Davis,§ and C. C. Schenck§

Department of Biochemistry SJ-70, University of Washington, Seattle, Washington 98195, and Department of Biochemistry, Colorado State University, Fort Collins, Colorado 80523

Received June 16, 1993; Revised Manuscript Received September 3, 1993®

ABSTRACT: The rates of the light-driven, electron-transfer reactions in the photosynthetic reaction center (RC) of *Rhodobacter sphaeroides* are examined in mutant strains in which tyrosine (M)210 is replaced by phenylalanine, isoleucine, or tryptophan. The spectra of the absorbance changes between 700 and 975 nm, following excitation by 0.6-ps pulses at 605 nm, are analyzed globally by singular value decomposition. The spectra measured at room temperature are interpreted in terms of a model in which the excited bacteriochlorophyll dimer (P*) transfers an electron to a bacteriopheophytin (H_L) with time constants of 3.5 ± 0.3, 10.5 ± 1.0, 16 ± 2, and 41 ± 4 ps in wild-type RCs and the Phe, Ile, and Trp mutants, respectively, and an electron then moves from H_L^- to a quinone (Q_A) with a time constant of 0.16 ns in wild-type RCs, 0.24 ns in the Phe mutant, and 0.20 ns in the Ile and Trp mutants. The first step speeds up with decreasing temperature in wild-type RCs, remains virtually unchanged in the Phe mutant, and slows down in the Ile and Trp mutants. At 80 K, the signals in the 850–975-nm region include an apparent shift of the stimulated emission or absorption spectrum of P*, with a time constant of 5 ps in the Ile mutant and 13 ps in the Trp mutant. Most of the electron transfer to H_L occurs with time constants of 55 and 155 ps in the Ile and Trp mutants, respectively, and probably occurs from the relaxed form of P*. Electron transfer from the initial state cannot be ruled out, however. Relaxations of P* are not resolved in wild-type RCs or the Phe mutant. The midpoint potential (E_m) of the P/P^+ redox couple is measured by an electrochemical technique; the E_m values are 500 ± 5, 530 ± 6, 533 ± 3, and 552 ± 10 mV for the wild-type and the Phe, Ile, and Trp mutant RCs, respectively. These values are corroborated by chemical titrations. The free energy change ($\Delta G°$) associated with formation of the $P^+H_L^-$ radical pair from P* also is determined by measuring the amplitude of fluorescence on the nanosecond time scale after blocking electron transfer from H_L^- to Q_A. The free energy of $P^+H_L^-$ is elevated by an amount comparable to that calculated from the increase in the E_m of P in the Ile mutant and by about 16 meV more than this in the Phe and Trp mutants. Nonadiabatic electron-transfer theory is used to relate the rate constant of the formation of $P^+H_L^-$ to $\Delta G°$. The altered temperature dependence of the reaction in the mutants cannot be explained adequately on the assumption that the mutations only alter the overall $\Delta G°$, but it can be accounted for by assuming that they also increase the free energy of an additional state ($P^+B_L^-$) that serves as both a kinetic and a virtual intermediate. The requisite increases in the free energy of $P^+B_L^-$ are greater than the measured changes in the free energy of $P^+H_L^-$. The $P^+Q_A^- \rightarrow PQ_A$ back-reaction speeds up with decreasing temperature in all four strains. At room temperature, this reaction has time constants of 0.105 ± 0.01, 0.100 ± 0.005, 0.13 ± 0.01, and 0.045 ± 0.005 s in the wild-type and the Phe, Ile, and Trp mutant RCs, respectively. The large acceleration in the Trp mutant cannot be explained simply in terms of the change in $\Delta G°$ for this reaction.

In reaction center complexes (RCs)[1] of purple photosynthetic bacteria, excitation of a bacteriochlorophyll dimer (P) results in a series of electron-transfer reactions along one of two symmetrically positioned pigment chains. The excited dimer (P*) transfers an electron to a bacteriopheophytin (H_L), forming a $P^+H_L^-$ radical pair. From H_L^-, an electron moves to a quinone (Q_A) and then to a second quinone (Q_B). One of the longstanding puzzles concerning the RC is the role of the additional bacteriochlorophyll molecule (B_L) that sits between P and H_L (Deisenhofer & Michel, 1989; Allen et al., 1987; Chang et al., 1986). Kinetic measurements by Holzapfel et al. (1990) suggested that a $P^+B_L^-$ radical pair is an intermediate in the initial electron-transfer reaction; other studies (Woodbury et al., 1985; Breton et al., 1986; Kirmaier & Holten, 1991; Kirmaier et al., 1991; Lockhart et al., 1990) have favored the view that $P^+B_L^-$ is not formed as a distinct intermediate and that B_L instead serves to couple the electronic wave functions of P and H_L by superexchange. That both mechanisms operate in parallel has also been suggested (Bixon et al., 1991; Chan et al., 1991b). Electrostatic calculations based on the crystal structure of *Rhodopseudomonas viridis* (Parson et al., 1990a,b) suggested that the energy of $P^+B_L^-$ may be low enough so that this state could be formed readily from P* and that the stabilization of $P^+B_L^-$ results in part from interactions with a nearby tyrosine residue, (M)Y210. Replacement of Tyr (M)210 by a less polar residue was expected to increase the energy of $P^+B_L^-$ and thus decrease the rate of electron transfer. The expected change in the rate and temperature dependence of the reaction was verified

† This work was supported by the National Science Foundation (DMB-9111599) and the National Institutes of Health (GM-38214, GM-48254, and Research Career Development Award GM-00536).

* Author to whom correspondence should be addressed.

‡ University of Washington.

§ Colorado State University.

® Abstract published in *Advance ACS Abstracts*, November 1, 1993.

[1] Abbreviations: EDTA, ethylenediaminetetraacetic acid; E_m, midpoint redox potential; RC, reaction center; SVD, singular value decomposition.

0006-2960/93/0432-12324$04.00/0

experimentally in RCs of *Rhodobacter sphaeroides* (Nagarajan et al., 1990; Finkele et al., 1990). Studies of additional mutant RCs of another purple bacterium, *Rhodobacter capsulatus*, suggested that, although polar residues at position (M)210 might interact favorably with B_L^-, such a residue at either (M)210 or (L)181 also can act to stabilize P^+ (Chan et al., 1991a).

In wild-type RCs, the rates of electron transfer from P^* to H_L, from H_L^- to Q_A, and from Q_A^- back to P^+ all increase with decreasing temperature. Classical theories of nonadiabatic electron-transfer processes (Marcus & Sutin, 1985) describe such "activationless" reactions as occurring when the free energy surfaces of the reactant and product states intersect at the most stable configuration of the reacting molecules. This occurs when the overall change in free energy in the reaction ($\Delta G°$) is equal, but opposite in sign, to the reorganization energy (λ), so that the activation energy ($[\Delta G° + \lambda]^2/4\lambda$) is zero. Mutations that raise the free energy of the product state should destroy this matching and convert the reaction to a process that requires thermal activation. In accord with this picture, replacement of Tyr (M)210 by isoleucine made the primary electron-transfer reaction markedly temperature-dependent (Nagarajan et al., 1990). Substitution by phenylalanine gave an intermediate situation, in which the rate was essentially independent of temperature. By contrast, charging $\Delta G°$ for electron transfer from Q_A^- back to P^+ has little effect on the temperature dependence of this more exothermic reaction (Gunner et al., 1986; Gunner & Dutton, 1989). The free energy of $P^+Q_A^-$ has been varied by substituting other quinones for the native ubiquinone (Gunner et al., 1986; Gunner & Dutton, 1989), by applying electrical fields (Franzen et al., 1990; Franzen & Boxer, 1993), and by mutations that modify the hydrogen bonding of the protein to the bacteriochlorophylls of P (Williams et al., 1992b).

The present article describes more extensive studies of the rates of the electron-transfer reactions $P^* \rightarrow P^+H_L^-$, $P^+H_L^- \rightarrow P^+Q_A^-$, and $P^+Q_A^- \rightarrow PQ_A$ in mutant RCs with Tyr (M)-210 replaced by phenylalanine, isoleucine, and tryptophan. The free energy gap between P^* and $P^+H_L^-$ is determined in each strain by measuring the delayed fluorescence from $P^+H_L^-$ after blocking electron transfer to Q_A. The free energy changes associated with the $P^+Q_A^- \rightarrow PQ_A$ back-reaction are investigated by measuring the midpoint redox potential (E_m) of the P/P^+ couple. Equipped with knowledge of the free energy gaps, we can examine various phenomenological models for the electron-transfer reactions. We also explore relaxations of P^* that become detectable when the lifetime of the excited state is extended.

MATERIALS AND METHODS

Oligonucleotide site-directed mutants were constructed as described by Nagarajan et al. (1990), and reaction centers were prepared according to standard procedures (Woodbury et al., 1985; Nagarajan et al., 1990). Wild-type RCs were obtained both from *Rb. sphaeroides* strain WS-231 and from the carotenoidless strain R-26.

For picosecond absorption measurements, RCs were suspended in 10 mM Tris-HCl, 0.1% lauryldimethylamine oxide (v/v), and 10 mM EDTA at pH 8.0, and the sample concentration was adjusted to make $A_{850nm}^{1mm} \approx 1.4$. For low-temperature measurements, glycerol was added to a concentration of 60% (v/v). The picosecond spectrophotometer was as described (Nagarajan et al., 1990), except for a longer translation stage that allowed delays of up to 1.5 ns between the pump and probe flashes. The 605-nm excitation pulse excited less than 20% of the sample in the illuminated region. Between 100 and 150 time-resolved difference spectra extending from about 700 to 1000 nm were collected for each sample.

The time-resolved difference spectra were analyzed by singular value decomposition (SVD). In SVD, an $m \times n$ data matrix **A**, where the number of rows m is greater than or equal to the number of columns n, is factored into the product of an $m \times n$ matrix **U**, an $n \times n$ diagonal matrix **S** with positive or zero elements, and the transpose of an $n \times n$ orthogonal matrix **V**:

$$\mathbf{A} = \mathbf{USV}^T \quad (1)$$

This decomposition is almost always unique (Press et al., 1989). In the present application, we have n spectra, each corresponding to a particular time delay between the pump and probe pulses and including absorbance measurements at m wavelengths. SVD gives a **U** matrix, in which each column constitutes a basis spectrum. There are n such basis spectra, each spanning the m wavelengths. Each column of the **V** matrix represents the time course of the amplitude of the corresponding basis spectrum, and the elements of **S** represent the weightings of the basis spectra in the observed spectra. The value of S_{ii} decreases monotonically as i increases from 1 through n. Usually only the first few values of S_{ii} are significantly different from zero; the rest represent noise. The observed signal thus can be reconstructed accurately by retaining only the first few columns of **U** and the first few columns of **V**. This method affords a way to filter out noise from the data objectively without significantly distorting the signal. Moreover, the problem of evaluating kinetics at numerous wavelengths is reduced to one of simultaneously fitting a small number of kinetic traces (typically the first four or five columns of **V**). This contrasts with more conventional "global analysis" methods, in which the time course curves can number in the tens or hundreds because there is a separate curve for each wavelength. Unlike most other methods of data analysis, the first step in SVD (factoring the data array **A** as in eq 1) is independent of any kinetic models that are used later in the analysis.

The set of kinetic traces resulting from SVD were fit globally by nonlinear least-squares to a sum of exponentials convoluted with the cross-correlation $E(\tau)$ of the excitation and probe pulses. For the ith column of the **V** matrix,

$$V_i(t) = \int_0^t E(\tau) \sum_{j=1}^{J} a_{ij} e^{-k_j(t-\tau)}\, d\tau \quad (2)$$

where a_{ij} is the amplitude of the jth decay component. The absorption difference spectrum associated with each exponential decay component is given by

$$A_j(\lambda) = \sum_{i=1}^{I} U_i(\lambda) S_{ii} a_{ij} \quad (3)$$

where I is the number of significant components obtained from the SVD analysis and J is the number of exponential components (Hofrichter et al., 1985). Finally, by assuming a particular kinetic model for the overall reaction and relating the microscopic rate constants of the individual steps in the scheme to the k_j's, one can calculate the difference absorption spectrum for the formation of each intermediate (Holzapfel et al., 1990). $E(\tau)$ in eq 2 was obtained by fitting the initial rise kinetics of the bleaching at 850 nm to the function $\alpha \tanh(\beta(\tau - \tau_0))$, with α, β and τ_0 as adjustable parameters. This procedure assumes that the cross-correlation of the excitation and probe pulses has a $\mathrm{sech}^2(\tau)$ shape and that the exci-

tation causes an instantaneous bleaching on the blue side of the 865-nm absorption band. Although the latter assumption is not rigorously valid, the error probably has little effect on the analysis of kinetic components with time constants greater than the widths of the pulses. The $E(\tau)$ functions used to deconvolute the results for the Trp mutant were obtained from data collected on the same day with wild-type RCs. This was done to minimize distortions resulting from the decay of P* to the ground state in the mutant RCs (see below).

Kinetic components that are fast relative to the width of the probe pulse are likely to be distorted by group-velocity dispersion (chirping) of the probe. We tested the SVD procedure with simulated, noisy data convoluted with an excitation function that included chirping comparable to that of the experimental data. Inclusion of the chirp added one additional significant column to both **U** and **V**, which required an additional exponential term in eq 2. The time constant of this term was always much less than 0.1 ps. A similar, very fast component with a relatively small integrated weight was obtained in all of the analyses of experimental data. It is omitted from the results reported below.

Delayed fluorescence was measured by time-correlated single-photon counting as described by Woodbury and Parson (1984). For these measurements, RCs were suspended in 50 mM Tris-HCl (pH 8.0), 0.05% (v/v) Triton X-100, and 1 mM EDTA. The RC concentration was adjusted so that, at the excitation wavelength (600 nm), A^{1cm} was typically 0.2. The endogenous ubiquinone was reduced by the addition of 50 μM sodium dithionite after the sample had been deoxygenated by bubbling with N_2. Excitation of the sample was kept weak (<10 mW cm^{-2}), so that even under the high repetition rate of the excitation pulses (800 kHz), less than 5% of the sample was in the P^+ state. The irradiance level used was well within the region where the fluorescence depended linearly on the excitation intensity. The excitation beam was circularly polarized with a quarter-wave plate to minimize any effects of fluorescence anisotropy decay. Fluorescence emitted normal to the excitation was detected, through a 915-nm interference filter with a 10-nm bandwidth, by a photomultiplier with an S-1 photocathode. Peak counts of approximately 20 000 photons/channel were collected. Before and after each measurement with an RC sample, the instrument response function was measured, at the same wavelength as the sample fluorescence (915 nm), by detecting the fluorescence of the laser dye DQOCI (1,3′-diethyl-4,2′-quinolyloxadicarbocyanine iodide) dissolved in methanol. The fluorescence lifetime of this dye, estimated to be <3 ps (Mourou & Sizer, 1982), is much shorter than the instrument response time of ~1 ns. If the signals showed significant time shifts during the measurement, they were rejected and the experiment was repeated on a fresh sample.

Fluorescence data were fit by nonlinear least-squares to a convolution of the instrument-response function and a decay function. The decay function was the sum of an instantaneous component (prompt fluorescence) and a two- or three-exponential decay with a variable time shift between the instrument-response and RC emission curves.

The decay kinetics of $P^+Q_A^-$ was measured from absorbance changes at 425 nm due to the formation and decay of P^+, following excitation with flashes lasting about 20 ns (Blankenship & Parson, 1979). To block electron transfer to Q_B, approximately 1 mM *o*-phenanthroline was added from a solution in ethanol. The intensity of the excitation light was attenuated so that the change in the transmitted probe light intensity was <5%. For low-temperature measurements, glycerol was added to a final concentration of 60% (v/v).

Redox titrations of P were carried out in a thin-layer electrochemical cell similar to that described by Moss et al. (1991), with a home-built potentiostat of the adder type (McKubre & Macdonald, 1984). The working electrode was a gold mesh with 120 or 333 lines/in. (Buckbee-Mears Inc., St. Paul, MN), which was coated with a modifier to prevent adherence and denaturation of the protein and promote electron transfer. Either 1,4-dithiobipyridine (Moss et al., 1991; Taniguchi et al., 1982) or pyridine-4-carboxaldehyde thiosemicarbazone was used as a modifier, with equivalent results. The counter electrode was a platinum wire, and the reference was either calomel or Ag/AgCl. The optical path length of the cell was ~10 μm. For the titrations, RCs were suspended in 20 mM Tris-HCl (pH 8.0), 0.1% (v/v) Triton X-100, and 60 mM KCl. The sample was concentrated in a pressure cell to $A^{1cm}_{850nm} \approx 10$, and 0.15 mM potassium tetracyanomono(1,10-phenanthroline)ferrate(II) tetrahydrate, synthesized according to the procedure of Schilt (1960), was added as an electron-transfer mediator. Its higher E_m (0.61 V vs NHE; Schilt & Cresswell, 1966) makes this a better mediator than $K_3Fe(CN)_6$ for mutant RCs in which the E_m of P/P^+ is elevated. The oxidation state of P was monitored by the absorbance at 865 nm. The reversibility of the titration was checked by oxidizing and re-reducing the sample in the same experiment, and the E_m was extracted by a nonlinear least-squares fit of the titration curve to the Nernst equation. The titration method was checked by determining the E_m of cytochrome *c*; the measured value (248 ± 2 mV) agreed well with the published value (Moss et al., 1990).

We also performed redox titrations by chemically oxidizing and re-reducing the RCs. For these experiments, RCs suspended in 10 mM Tris-HCl, 1 mM EDTA, and 0.05% Triton X-100 at pH 8.0 were treated with sodium dithionite to ensure complete reduction, and excess dithionite was removed by dialysis. Redox mediators were then added to final concentrations of 3.5 μM RC protein, 0.75 mM potassium ferricyanide, and 0.75 mM hydrogen tetracyanomono(1,10-phenanthroline)ferrate(III) dihydrate (Schilt, 1960), so that P was completely oxidized as judged from the loss of the 865-nm absorption band. The samples were kept on ice and titrated with fresh dithionite solution. The potential of each aliquot was recorded with a Beckman Φ70 pH meter fitted with a platinum electrode (Orion Research). Complete re-reduction restored the 865-nm absorption band to 94–100% of its original value.

RESULTS

Absorption Spectra. The absorption spectra of two of the mutant RCs in the near-IR region are shown in Figure 1. Also shown for comparison is the absorption spectrum of reaction centers of the carotenoidless wild-type strain, R-26. The 802-nm bacteriochlorophyll band of wild-type RCs is red-shifted to 807 nm in all of the mutants. The 865-nm absorption band of P is shifted to 868 nm in the Phe (not shown) and Trp mutants and to 871 nm in the Ile mutant. These shifts are relatively small. For comparison, the 865-nm band shifts to the red by about 2.5 nm for every 20-deg cooling between 300 and 100 K (Kirmaier & Holten, 1988).

Kinetics of Charge Separation and Relaxations of P.* The absorbance changes caused by excitation with flashes lasting about 0.6 ps were measured at several temperatures with each of the bacterial strains. Because the kinetics of the initial electron-transfer step in the wild-type and Ile and Phe mutant RCs have been discussed before, we will describe the results obtained with the Trp mutant in greatest detail.

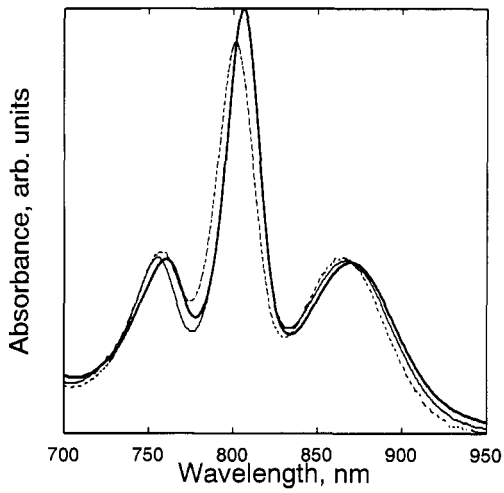

FIGURE 1: Absorption spectra of wild-type (broken line), and (M)-Y210W (thin solid line), and (M)Y210I (thick solid line) RCs in 20 mM Tris-HCl and 0.1% (v/v) lauryldimethylamine *N*-oxide at pH 8.0 and 295 K. The spectrum of the Phe mutant (not shown) was very similar to that of the Trp mutant.

Singular value decomposition of time-resolved spectra obtained with the Trp mutant at room temperature could be adequately described with four significant kinetic components, with time constants of 0.4 ± 0.15, 33 ± 2, and 200 ± 20 ps and >1.5 ns. (As mentioned in Materials and Methods, we neglect a small, faster component that probably results from the group-velocity dispersion in the probe pulse.) Figure 2D shows the amplitude spectra associated with these components. Inclusion of an additional kinetic component improved the fit only marginally. The amplitude spectra are combinations of the absorption spectra of intermediates whose individual contributions depend on the actual reaction scheme. To relate the amplitude spectra and time constants to physical states of the RC, we assumed a kinetic model with four transient states connected by a linear sequence of irreversible reactions, as shown in Scheme I. The difference spectra for formation of states I–IV from the ground state were then calculated as described in Materials and Methods. These model-dependent spectra are shown in Figure 2E. The alternative model obtained by interchanging the order of the 33- and 0.4-ps steps led to similar spectra for states III and IV, but gave spectra that seemed physically implausible for the two earlier states. (The calculated bleaching of one or more of the absorption bands was unrealistically large relative to the original absorption spectrum.)

Scheme I

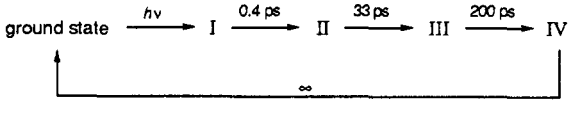

Because the 605-nm excitation flashes that we used excited B_L and B_M in addition to P, the 0.4-ps kinetic component could include energy transfer from the other bacteriochlorophylls to P. In agreement with this expectation, the amplitude spectrum of this component includes decay of an initial bleaching near 800 nm and a growing bleaching in the 865-nm band of P (Figure 2D,E). The fast component could also include contributions from the sub-picosecond kinetic transient that Holzapfel et al. (1990) have described for wild-type RCs. Similar components with time constants of approximately 0.5 ps were seen also in wild-type RCs and the Phe and Ile mutants. They were too fast to be analyzed reliably because their spectra and time constants could be distorted by the procedure that we used to deconvolute the instrument function, $E(\tau)$, in eq 2.

The calculated spectra for states III and IV shown in Figure 2E are similar to those described previously for $P^+H_L^-$ and $P^+Q_A^-$, respectively (Kirmaier et al., 1985; Woodbury et al., 1985). The intermediate with a 33-ps lifetime (state II) exhibits bleaching of the 870-nm band of P, stimulated emission in the 900-nm region, and absorbance increases at wavelengths below 810 nm. Its spectrum closely resembles difference spectra measured at sub-picosecond times with wild-type RCs (Vos et al., 1992; Kirmaier & Holten, 1990). On the basis of these observations, we identify the 33-ps intermediate as P*. The sharp absorption feature at 807 nm can be rationalized by excitonic interactions of P with B_L and B_M: when P is excited, the absorption bands of B_L and B_M would recover the intensity that they lend to the bands at longer wavelengths (Parson & Warshel, 1987). However, absorption bands of the excited bacteriochlorophylls could also contribute to the absorbance changes in this region. The first excited singlet state of monomeric bacteriochlorophyll in solution has a broad absorption band to the blue of the ground state's Q_y band (Becker et al., 1991).

The amplitude of the bleaching in the 850-nm region is smaller in the difference spectra for $P^+H_L^-$ and $P^+Q_A^-$ than it is in the spectrum for P* (Figure 2E). No such loss of signal near 850 nm is seen in wild-type RCs (Kirmaier et al., 1985; Woodbury et al., 1985; Breton et al., 1986) or in the other mutant strains studied here (data not shown). In these cases, the main difference between the spectra of P* and $P^+H_L^-$ and $P^+Q_A^-$ in the region of the long-wavelength band is confined to wavelengths of >860 nm and can be ascribed reasonably to stimulated emission from P*. It is possible that the stimulated-emission spectrum of P* is broader in the Trp mutant than in the other strains. However, the width of the long-wavelength absorption band of P is similar in all of the strains (Figure 1), and the fluorescence emission spectra of P* are also virtually identical (data not shown). Hence, the stimulated-emission spectra should be similar for all of the strains. A more plausible explanation of the observed difference is that the quantum yield of $P^+H_L^-$ is diminished in the Trp mutant by a parallel decay of P* to the ground state. Judging from the ratio of the initial and long-lived absorbance changes around 850 nm, the yield of $P^+H_L^-$ is 80 ± 2%. When combined with the observed time constant of 33 ± 2 ps for the transition from state II to state III, this yield is consistent with time constants of 41 ± 4 ps for $P^* \rightarrow P^+H_L^-$ and 170 ± 30 ps for $P^* \rightarrow P$ (Scheme II). The decay of P* to the ground state appears to be significantly slower in the Ile mutant, where electron transfer occurs with a quantum yield near unity (Nagarajan et al., 1990). The observed electron-transfer time constant of 16 ± 2 ps at room temperature puts a lower limit of ~300 ps for $P^* \rightarrow P$ in that strain.

Scheme II

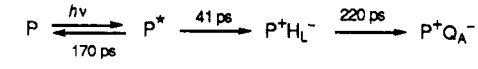

Time-resolved spectra obtained with wild-type RCs and the Phe and Ile mutants were analyzed by SVD in the manner described for the Trp mutant. Table I gives the rate constants for the electron-transfer steps $P^* \rightarrow P^+H_L^-$ and $P^+H_L^- \rightarrow P^+Q_A^-$ for all the strains. At room temperature, the data were always satisfactorily fit by using a single-exponential decay component for each step. The time constants for the first step in the wild-type strain and the Phe and Ile mutants are, within experimental error, the same as those measured

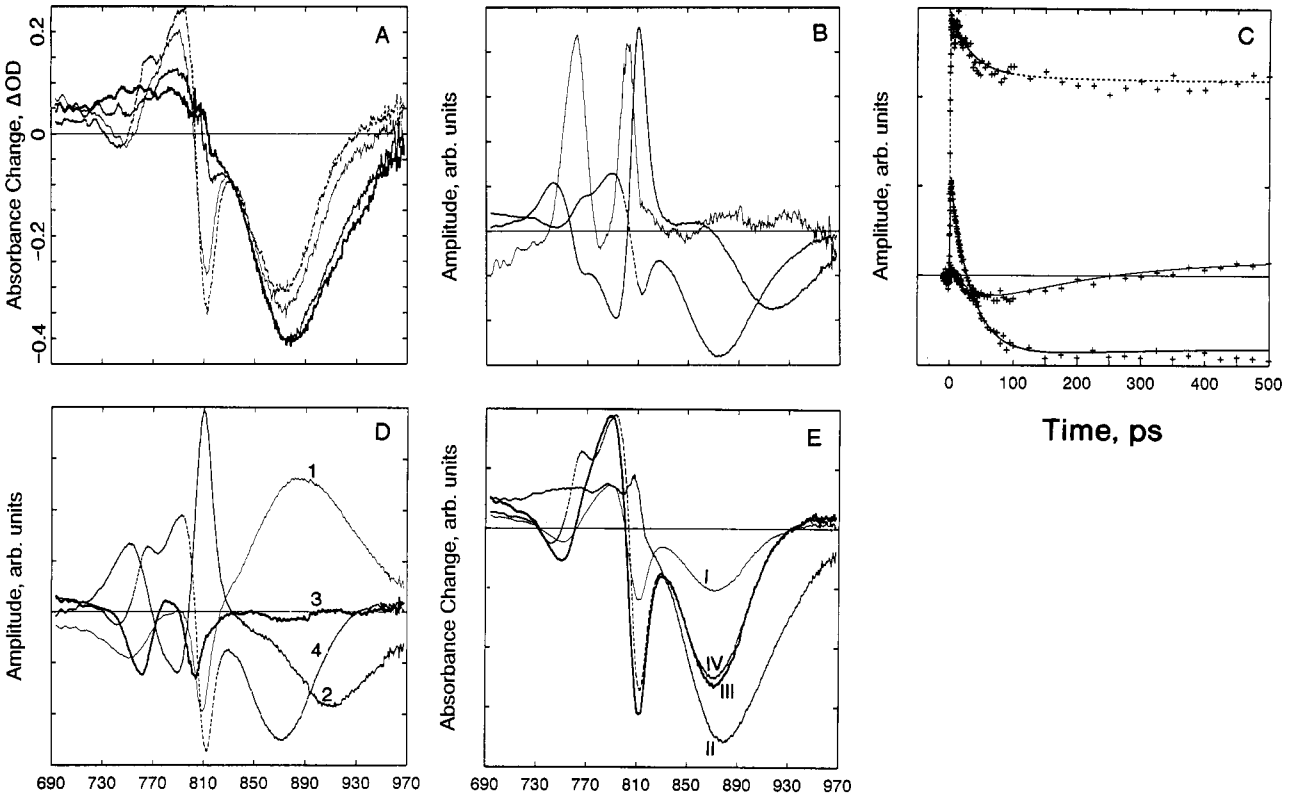

FIGURE 2: Initial, intermediate, and final results from a combination of SVD, global kinetic analysis, and kinetic modeling for the Trp mutant at 295 K. (A) Representative absorbance difference spectra for pump/probe time delays of 1.6, 10, 50 ps and 0.5 ns. The decreasing line thickness of the curves signifies increasing time delay. (B and C) First three components from SVD analysis with relative singular values of 1., 0.28, and 0.05 for the dashed, thick, and thin lines, respectively. The basis spectra are shown in B, and the corresponding decay curves (points) are shown in C; also shown in C are the global, nonlinear least-squares fits to the data (lines). (D) Amplitude spectra, generated from the data shown in B and C, of decay components with lifetimes of (1) 0.4, (2) 34, and (3) 195 ps and (4) ∞. (E) Calculated difference spectra for the formation of the four states in Scheme I. In all panels, the straight horizontal line is the zero of the ordinate scale.

previously by following the decay of the stimulated emission at single wavelengths (Nagarajan et al., 1990). The time constants for the second step are the same in the Ile and Trp mutants and are somewhat longer than those in wild-type RCs. In the Phe mutant, the rate of quinone reduction is lower still.

As described previously (Woodbury et al., 1985; Fleming et al., 1988; Nagarajan et al., 1990), the initial charge-separation reaction in wild-type RCs speeds up with decreasing temperature. In the Phe mutant, the rate is essentially independent of temperature between 100 and 295 K. The kinetics in both the Ile and Trp mutants become much slower at low temperatures. For the Trp mutant, SVD analysis of the absorbance changes and stimulated emission in the 830–950-nm region at 80 K revealed three significant kinetic components, with time constants of 13 and 155 ps and >1.5 ns. A fit of the decay of the stimulated emission at individual wavelengths gave similar results; at 930 nm, for example, such a fit returned time constants of 12 and 200 ps and >1.5 ns. Figure 3A shows the amplitude spectra of the three components in the SVD analysis. Except for the red shift resulting from the lower temperature, the amplitude spectrum of the 155-ps component resembles that of the 33-ps component at room temperature (Figure 2D). This component probably represents much of the electron transfer to H_L. The amplitude spectrum of the 13-ps component is decidedly different and suggests a separate relaxation in which the stimulated emission shifts to shorter wavelengths or an underlying absorption band shifts to longer wavelengths.

Scheme III

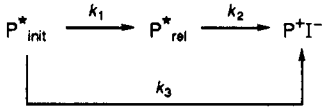

Model-dependent spectra for the states preceding and following the putative relaxation were calculated by adopting the general scheme outlined in Scheme III. Here P^*_{init}

Table I: Time Constants for the Electron-Transfer Reactions[a]

strain	$P^*H_L \rightarrow P^+H_L^-$ (ps) 295 K	$P^*H_L \rightarrow P^+H_L^-$ (ps) 80 K	$P^+H_L^- \rightarrow P^+Q_A^-$ (ps)	$P^+H_L^- \rightarrow PH_L + {}^3P$ (ns)	$P^+Q_A^- \rightarrow PQ_A$ (ms)
wild type	3.5 ± 0.3	1.7 ± 0.2	160 ± 20	9.2 ± 1.0[b]	105 ± 10
(M)Y210F	10.5 ± 1.0	10.5 ■ 1.0	240 ± 20	13.0 ± 1.0	100 ± 5
(M)Y210I	16 ± 2	55 ± 5	200 ± 20	10.3 ± 1.0	130 ± 10
(M)Y210W	41 ± 4	155 ± 10	200 ± 20	9.7 ± 1.0	45 ± 5

[a] Temperature was 295 K except as indicated. The stated uncertainties are estimates based on several measurements with each strain. [b] Includes evolution into triplet states in addition to decay to the ground state (see text).

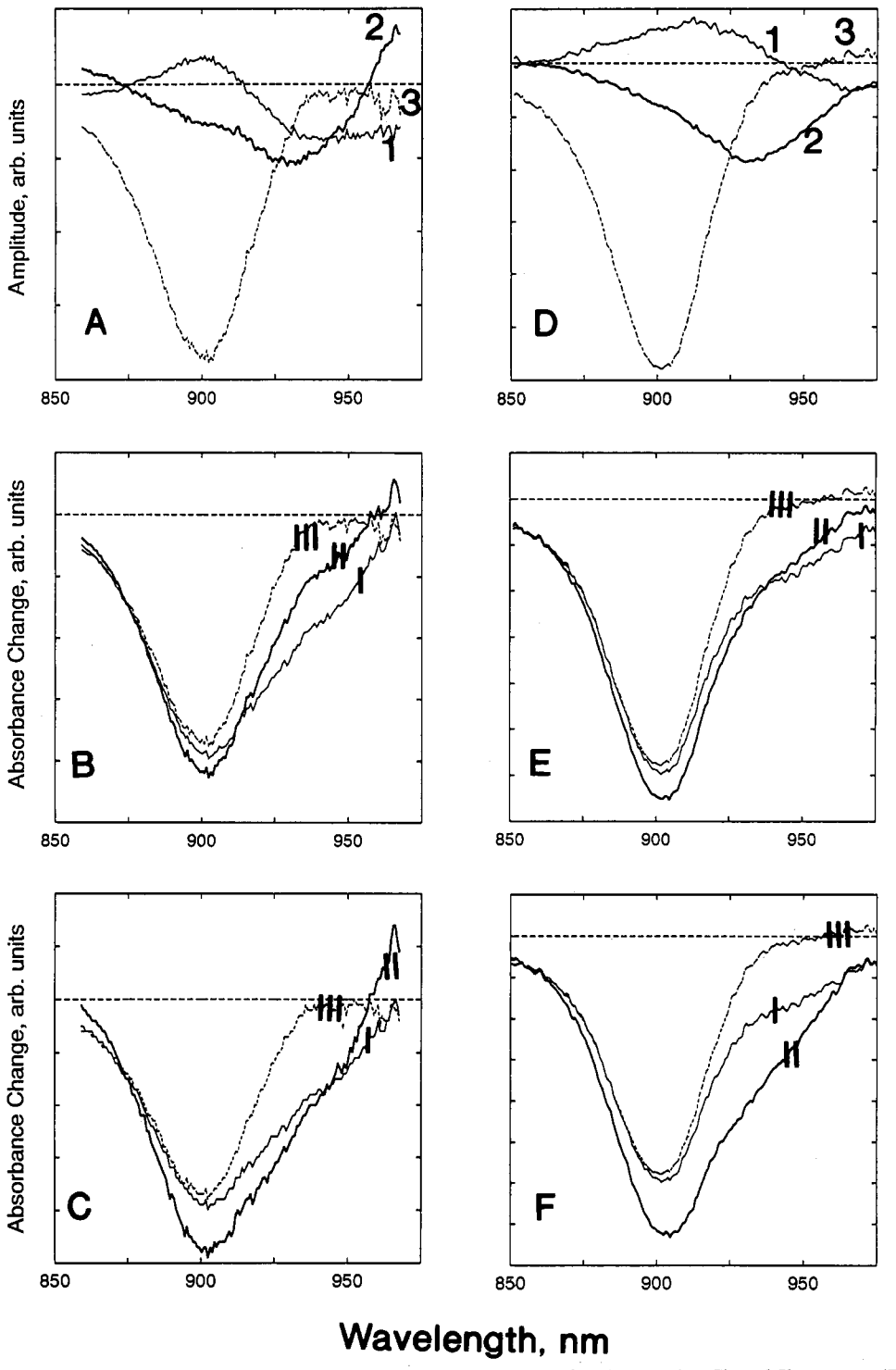

FIGURE 3: Amplitude spectra and model-dependent difference absorbance spectra for the Trp (A–C) and Ile mutant (D–F) RCs at 80 K. Only the spectral region between 850 and 975 nm was considered in the analysis. Labels I, II, and III refer to P^*_{init}, P^*_{rel}, and P^+I^-, respectively. (A) Amplitude spectra of the three resolved kinetic components for the Trp mutant [time constants (1) 13 ps, (2) 155 ps, and (3) ∞]. (B) Calculated difference spectra for the formation of the three states in Scheme III with $k_1 = (13\ ps)^{-1}$, $k_2 = (155\ ps)^{-1}$, and $k_3 = 0$. (C) Calculated difference spectra for the formation of the three states in Scheme III with $k_1 = (25\ ps)^{-1}$, $k_2 = (155\ ps)^{-1}$, and $k_3 = (29\ ps)^{-1}$. (D) Amplitude spectra of the three resolved kinetic components for the Ile mutant [time constants (1) 5 ps, (2) 55 ps, and (3) ∞]. (E) Calculated difference spectra for the formation of the three states in Scheme III with $k_1 = (5\ ps)^{-1}$, $k_2 = (55\ ps)^{-1}$, and $k_3 = 0$. (F) Calculated difference spectra for the formation of the three states in Scheme III with $k_1 = (2.5\ ps)^{-1}$, $k_2 = (55\ ps)^{-1}$, and $k_3 = (2.5\ ps)^{-1}$.

represents an initial form of P* (or the mixture of P*, B_L*, and B_M* created by the 605-nm excitation), which relaxes with rate constant k_1 to an, as yet, uncharacterized excited state, P^*_{rel}. P^+I^- represents $P^+H_L^-$ or a mixture of $P^+H_L^-$ and $P^+Q_A^-$, which are spectroscopically indistinguishable in the 830–950-nm region of the spectrum. Because the measurements provide only two time constants, the ratio k_1/k_3 is not determined uniquely. We can, however, set $k_1 + k_3 = (13\ ps)^{-1}$ and $k_2 = (155\ ps)^{-1}$, because setting $k_2 = (13\ ps)^{-1}$ leads to an unphysically large bleaching in the calculated spectrum of P^*_{rel}. Figure 3B shows the spectra obtained by setting $k_1 = (13\ ps)^{-1}$ and $k_3 = 0$ and, thus, assuming that electron transfer to H_L occurs only from P^*_{rel}. The calculated difference spectrum corresponding to P^*_{rel} is similar to that of P^*_{init}, except that the apparent contribution from stimulated emission is smaller and is shifted to shorter wavelengths. In the opposite limit, where $k_3 \gg k_1$, the calculated bleaching associated with P^*_{rel} is unphysically large (not shown). Figure

3C shows spectra for an intermediate situation, $k_3 \approx k_1$. Here the areas under the stimulated-emission regions are similar in the spectra for P^*_{init} and P^*_{rel} and the emission again appears to be shifted to shorter wavelengths in P^*_{rel}, but P^*_{rel} has greater bleaching at wavelengths <900 nm.

Figure 3D–F shows the results of similar analyses of low-temperature data for the Ile mutant. The time constants measured with this strain were approximately 5, 55, and >200 ps (the longest time delay used in this case). The slower of the two resolved steps (55 ps) appears to include most of the decay of the stimulated emission. The time constant of this step is similar to the mean time constant of 50 ps obtained previously by using a stretched-exponential function to fit the decay of the emission at 935 nm (Nagarajan et al., 1990). As with the Trp mutant, the faster process (5 ps) suggests a separate relaxation in which the emission shifts to the blue. The model-dependent spectra calculated for states I and II in Scheme III have similar areas in the stimulated-emission region if we set $k_3 \ll k_1$ (Figure 3E); setting $k_3 \gtrsim k_1$ makes the calculated bleaching for P^*_{rel} considerably greater than that for P^*_{init} (Figure 3D). Thus, although the time constants differ in the Trp and Ile mutants, the data for both strains lead to physically plausible calculated spectra, as long as k_3 is in the range $0 \leq k_3 \lesssim k_1$. Evidently it is mainly P^*_{rel} that gives rise to $P^+H_L^-$ in both strains. The spectroscopic features of the relaxation are considered in the Discussion, where we also address the possibility that the multiphasic kinetics reflect heterogeneity of the RCs.

Measurements of the absorbance changes in the 760–830-nm region did not serve to clarify the nature of the relaxation, because they included overlapping contributions from both the initial charge separation and the secondary electron transfer to Q_A. In the Trp and Ile mutants, the initial electron-transfer reaction slows down with decreasing temperature, whereas the second reaction speeds up as it does in wild-type RCs. At temperatures below about 100 K, the two steps have similar kinetics and the fitting procedure is unable to resolve them reliably. However, judging from the spectra measured at room temperature (Figure 2), the secondary electron-transfer step makes little contribution to the signals in the 830–950-nm region (Figure 3).

No indications of relaxations of the stimulated-emission spectrum were obtained with wild-type RCs or with the Phe mutant. With the Phe mutant at 80 K, SVD analysis of the spectra in the stimulated-emission region provided a single decay component with a time constant of 10 ps, in agreement with the results of our earlier analysis at individual wavelengths (Nagarajan et al., 1990). Similar data for wild-type RCs at 100 K were fit well with a single time constant of 1.7 ± 0.2 ps.

In contrast to the situation at room temperature, the Trp mutant at low temperatures offered little evidence for direct decay of P* to the ground state. The bleaching on the blue side of the long-wavelength absorption band did not recover significantly during the lifetime of P*. This conclusion is relatively insensitive to the choice of the kinetic model used for analyzing the data (compare the spectrum of P^*_{init} with that of P^+I^- in either Figure 3B or C). The rate at which P* decays to the ground state thus appears to be strongly temperature-dependent. The 0.5-ps rise component seen at room temperature also could not be resolved at low temperatures with any of the strains. If energy transfer from the other bacteriochlorophylls to P were slowed at low temperatures, this component could possibly overlap (and obscure) the relaxation seen on the 5- or 13-ps time scales in the Ile and Trp mutants. However, we then would expect to see indications of the same process in the Phe mutant since the absorption and emission spectra of all of the strains are similar.

Free Energy and Recombination Kinetics of $P^+H_L^-$. Most of the fluorescence emitted by RC samples with unreduced Q_A decayed with lifetimes of less than 0.3 ns. The fluorescence from the mutant RCs was compared with that measured under identical conditions in wild-type RCs. The integrated amplitude of the prompt component was elevated by a factor of 2.7 ± 0.3 in the Phe mutant, 3.7 ± 0.4 in the Ile mutant, and 11 ± 1 in the Trp mutant. These ratios agree well with the ratios of the time constants of the initial electron-transfer reaction at 295 K.

The fluorescence from all of the strains also included weak components with longer lifetimes. The longest of these had a lifetime of ~2 ns and an emission spectrum that peaked near 800 nm. This component probably reflects trace amounts of free bacteriochlorophyll in the sample. Fluorescence with a lifetime of ~10 ns, which would be expected from RCs lacking Q_A (Schenck et al., 1982), was not detected with any of the unreduced RC samples, and the addition of small amounts of ubiquinone to the samples did not alter the results.

When electron transfer from H_L^- to Q_A is blocked by reduction of the quinone, the fluorescence includes delayed fluorescence with a multiphasic decay in addition to prompt emission similar in amplitude to the fluorescence from unreduced RCs. A major component of the delayed fluorescence decays with a time constant of approximately 10 ns, which probably reflects the decay of $P^+H_L^-$ by charge recombination (Schenck et al., 1982; Woodbury & Parson, 1984). At room temperature, about 70% of the singlet radical pair decays directly to the ground state; the remainder evolves into a triplet radical pair that collapses quickly to a local triplet state of P (Schenck et al., 1982; Ogrodnik et al., 1982; Boxer et al., 1983). The overall recombination times in the Phe, Ile, and Trp mutants are similar to those in wild-type RCs (Table I).

The delayed fluorescence from all of the strains also included a component with a time constant of about 3 ns. The measured lifetimes of this component were 2.6 ± 0.4, 3.4 ± 0.4, 2.3 ± 0.2, and 2.6 ± 0.2 ns in wild-type, (M)Y210F, (M)Y210I, and (M)Y210W RCs, respectively. Earlier components with lifetimes of 300–500 ps also were present, but they could not always be resolved reliably from the prompt fluorescence. Recent measurements with higher time resolution have shown that the delayed fluorescence can also include components with lifetimes of 100 ps or less (Williams et al., 1992a).

The multiphasic decay of the delayed fluorescence has been attributed to nuclear relaxation of the surrounding protein, subsequent to the formation of $P^+H_L^-$ (Woodbury & Parson, 1984; Goldstein & Boxer, 1989). If P* and $P^+H_L^-$ are assumed to be in thermal equilibrium within the time resolution of the measurements, the equilibrium constant can be calculated from the ratio of the amplitudes of the delayed and prompt fluorescences (Schenck et al., 1982; Woodbury & Parson, 1984). When measurements on the mutant and wild-type samples are made under identical conditions, differences in the initial amplitudes of the 10-ns component of the delayed fluorescence afford a measure of changes in the free energy gap between P* and the most relaxed form of $P^+H_L^-$:

$$\Delta\Delta G^\circ_{P^*\rightarrow P^+H^-} = k_B T \ln (a_m/a_{wt}) \qquad (4)$$

where a is the initial amplitude of the 10-ns fluorescence component, k_B is the Boltzmann constant, and the subscripts m and wt refer to mutant and wild-type samples, respectively. As shown in Table II, the standard free energy of $P^+H_L^-$ is increased in all of the mutants. We also calculated the

Table II: Free Energy Changes and E_m Values[a]

strain	$\Delta\Delta G^\circ_{P^*\rightarrow P^+H^-}$ partly relaxed	$\Delta\Delta G^\circ_{P^*\rightarrow P^+H^-}$ relaxed	$\Delta G^\circ_{P^*\rightarrow P^+H^-}$ partly relaxed	$\Delta G^\circ_{P^*\rightarrow P^+H^-}$ relaxed	$E_m(P/P^+)$
wild type	0	0	−170 ± 5	−203 ± 10	500 ± 5
(M)Y210F	21 ± 1	46.0 ± 0.5	−146 ● 5	−163 ● 10	530 ● 6
(M)Y210I	13 ± 1	31.5 ● 0.5	−152 ± 5	−175 ± 10	533.5 ± 2.5
(M)Y210W	48 ± 1	69.0 ± 0.5	−125 ± 5	−146 ± 10	552 ± 10

[a] Temperature was 295 K. Free energy values (means and standard deviations of the means of 2–4 measurements on each strain) are for $P^* \rightarrow P^+H_L^-$ and are given in millielectronvolts. The $\Delta\Delta G^\circ$'s are calculated relative to the wild-type strain by eq 4, using only the initial amplitude of the slow component of the delayed fluorescence ("relaxed" $P^+H_L^-$) or the sum of the intermediate and slow components ("partly relaxed" $P^+H_L^-$). The ΔG°'s are calculated by eq 5, using only the slow component ("relaxed" $P^+H_L^-$) or the sum of the intermediate and slow components ("partly relaxed" $P^+H_L^-$). E_m values (means and standard deviations of the means of at least four titrations for each strain) are given in millivolts with respect to H_2/H^+.

standard free energy for each individual bacterial strain with the expression,

$$\Delta G^\circ_{P^*\rightarrow P^+H^-} = k_B T \ln (a\tau/\alpha) \quad (5)$$

where α is the time integral of the prompt fluorescence and τ is the lifetime of P* in unblocked RCs (3.5, 10.5, 16, and 33 ps for wild-type and Phe, Ile, and Trp mutant RCs, respectively). This method led to values of $\Delta\Delta G^\circ_{P^*\rightarrow P^+H^-}$ similar to those obtained via eq 4 (see Table II), but the results are less reliable because of the difficulty of resolving prompt fluorescence from the fastest components of the delayed fluorescence.

$\Delta\Delta G^\circ_{P^*\rightarrow P^+H^-}$ and $\Delta G^\circ_{P^*\rightarrow P^+H^-}$ values for an earlier, unrelaxed form of $P^+H_L^-$ can be obtained from the sum of the initial amplitudes of the 3- and 10-ns components. The calculated values are given in Table II. The trend in the values among the different strains is similar to that for the more relaxed state, although the differences are smaller. Measurements with faster time resolution put still earlier unrelaxed forms of $P^+H_L^-$ within 120 meV of P* (Williams et al., 1992a). Figure 4 shows a plot of the rate constant for the formation of $P^+H_L^-$ from P* as a function of $\Delta G^\circ_{P^*\rightarrow P^+H^-}$ for the relaxed form of $P^+H_L^-$.

Free Energy and Recombination Kinetics of $P^+Q_A^-$. $P^+Q_A^-$ decay curves were analyzed by fitting the absorbance changes to a single-exponential expression. The decay is slightly slower in the Ile mutant than in wild-type RCs, slightly faster in the Phe mutant, and much faster in the Trp mutant (Table I). Figure 5 shows that the temperature dependence of the rate is similar in all of the strains. Although Kleinfeld et al. (1984) have shown that the decay is nonexponential at 77 K, the signal-to-noise ratio in our measurements was not high enough to reveal nonexponential kinetics. Hence, the decay time constants reported here for low temperatures are probably mean values.

Figure 6 shows representative electrochemical redox titrations of P. Each curve represents a complete oxidation–reduction cycle. There was little hysteresis in the titrations. The E_m values are increased by 30–50 mV in the mutant strains, with the Trp mutant exhibiting the greatest effect (Table II). The measured values depended to some extent on the ionic strength of the solution, but the dependence was similar for all of the strains (P. Bowers and V. Nagarajan, unpublished results). E_m values determined by chemical titrations for the wild-type and Phe and Ile mutant RCs agreed with the results of the electrochemical titrations within the uncertainty limits. The E_m value for the Trp mutant was slightly (~8 mV) more positive with the chemical method.

The free energy gaps between $P^+Q_A^-$ and the ground state ($\Delta G^\circ_{P^+Q^-\rightarrow PQ}$ in the mutant strains can be estimated by starting with the value for wild-type RCs (520 meV) (Arata & Parson, 1981) and assuming that the free energies of $P^+Q_A^-$ are increased in the mutants in proportion to the changes in the E_m of P. The latter assumption seems reasonable as a first approximation, considering that the sites of the amino acid substitutions are adjacent to P but are some 20 Å from Q_A. Figure 4 shows the rate constant for the reaction $P^+Q_A^- \rightarrow PQ_A$ in the four strains as a function of the calculated free energy gap.

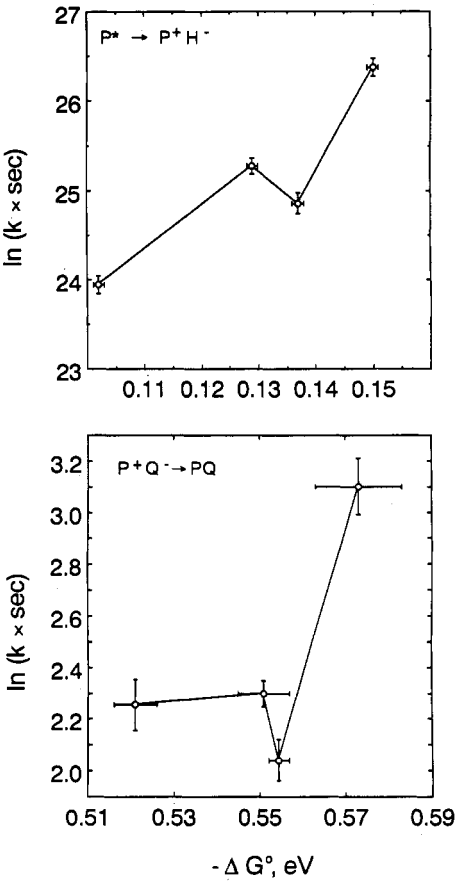

FIGURE 4: Top panel: Rate constant for the reaction $P^* \rightarrow P^+H_L^-$, as a function of the standard free energy change ($\Delta G^\circ_{P^*\rightarrow P^+H^-}$). The ΔG° for wild-type RCs was taken to be −0.15 eV, and the $\Delta\Delta G^\circ$ values for the relaxed form of $P^+H_L^-$ (Table II) were used to calculate ΔG° for the mutants. Bottom panel: Rate constant for the reaction $P^+Q_A^- \rightarrow PQ_A$, as a function of the standard free energy change ($\Delta G^\circ_{P^+Q^-\rightarrow PQ}$). The ΔG° for the wild-type RCs is −0.52 eV; the values for the mutants and the wild type were assumed to differ in parallel with the changes in the $E_m(P/P^+)$ values (Table II).

The free energy changes associated with electron transfer from H_L^- to Q_A ($\Delta G^\circ_{P^+H^-\rightarrow P^+Q^-}$) can be estimated from the calculated free energies of $P^+H_L^-$ and $P^+Q_A^-$. However, the calculated differences between the mutant and wild-type RCs are relatively small and are comparable to the uncertainties in the measurements. This is in accord with the observation that the rates of electron transfer from H_L^- to Q_A are little affected in the mutants (Table I).

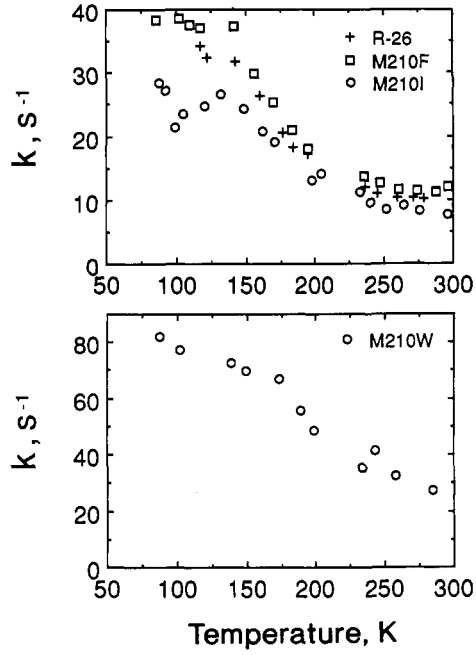

FIGURE 5: Rate constants for the reaction $P^+Q_A^- \rightarrow PQ_A$, as a function of temperature.

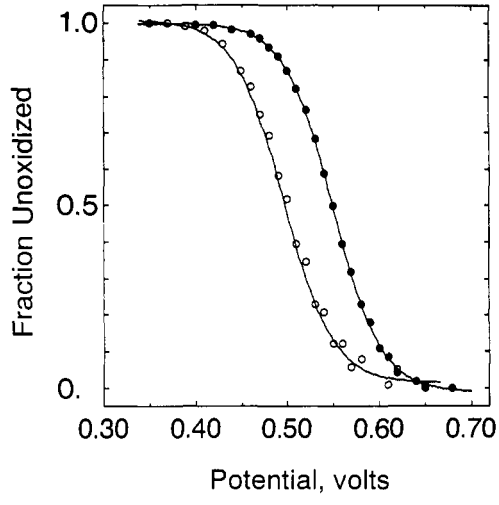

FIGURE 6: Electrochemical redox titrations of P in wild-type (○) and the Trp mutant (●). Each curve includes both an oxidative and a reductive titration. The lines are best fits to the Nernst equation with E_m values of 0.50 eV (with respect to the standard hydrogen electrode) for the wild-type RCs and 0.55 eV for the Trp mutant.

DISCUSSION

Replacement of Tyr (M)210 by either Phe, Ile, or Trp raises the E_m of P, increases the standard free energy of $P^+H_L^-$, slows the initial charge-separation reaction ($P^* \rightarrow P^+H_L^-$), and changes the temperature dependence of this reaction. The second electron-transfer reaction ($P^+H_L^-Q_A \rightarrow P^+H_LQ_A^-$) and charge recombination within $P^+H_L^-$ are not greatly affected, but the charge recombination of $P^+Q_A^-$ is sped up unexpectedly in the Trp mutant. The slowing of the initial electron-transfer reaction in the Trp and Ile mutants also opens an experimental window on relaxations of P* that are difficult to examine in wild-type RCs.

*Relaxations of P**. At room temperature, the decay kinetics of the stimulated emission from P* was described well by a single-exponential function, and similar rate constants were obtained either by SVD analysis or by fitting the signal at individual wavelengths. Similar results were obtained at low temperatures in the wild-type strain and the Phe mutant, but the kinetics in the Ile and Trp mutants were more complex. In previous work on the Ile mutant (Nagarajan et al., 1990), we noted that the emission appeared to shift to shorter wavelengths during the first few picoseconds after excitation. However, the decay kinetics was nonexponential, even at wavelengths near the peak of the stimulated-emission spectrum where one might expect the signal to be insensitive to small shifts of the spectrum. In the present work, we found that SVD dissected the kinetics into two exponential components with distinctly different amplitude spectra (Figure 3A,D). The slower component accounts for most of the decay of the stimulated emission in both mutant strains, and we interpret this component as reflecting electron transfer to H_L. The faster component appears to reflect a different type of relaxation involving a shift of the emission or an underlying absorption band. There may also be a change in the overall amplitude of the stimulated emission, but the direction and magnitude of this effect are difficult to judge because the calculated spectra depend on the assumed ratio of k_1 to k_3 in Scheme III (Figure 3B,C).

A time-dependent shift of the emission to higher energies would be counterintiutive. The possible change in the amplitude of the stimulated emission is also problematic. However, the factors that contribute to the emission amplitude are not well understood. If the relaxed and unrelaxed states represent different mixing of excitonic and charge-transfer states of P, there is no reason *a priori* to expect their emission strengths to be the same. For example, a decrease in the orbital overlap between the two bacteriochlorophylls of P would shift the emission spectrum to shorter wavelengths and increase the strength of the emission. Perhaps significantly, the emission amplitude appears to be considerably greater in a photochemically inactive mutant of a related bacterium, *Rb. capsulatus* (Vos et al., 1993).

The theoretical cross-section for stimulated emission can be estimated from the spontaneous fluorescence spectrum if one knows the fluorescence quantum yield (ϕ) and lifetime (τ) (Becker et al., 1991). Using the fluorescence spectrum of wild-type RCs at 295 K (Woodbury & Parson, 1984), $\phi = 4 \times 10^{-4}$ (Zankel et al., 1968), and $\tau = 3.5$ ps, the calculated cross-section at 910 nm is approximately the same as the absorption cross-section at 865 nm ($\sim 4.3 \times 10^{-16}$ cm^2). A similar relationship should hold in the mutant strains and should be maintained at low temperatures. The observed amplitude of the (P* – P) difference spectrum in the 910-nm region is smaller than would be expected, on the basis of the calculated stimulated-emission cross-section, by a factor of about 2 at 295 K and 3 at 80 K [Figures 2 and 3; see also Woodbury et al. (1985)]. This suggests that the P* spectra include an opposing contribution from excited-state absorption, as appears to be the case with bacteriochlorophyll *in vitro* (Becker et al., 1991). Alternatively, P* might undergo an unresolvably fast relaxation to a state with a lower emission cross-section.

Another possible interpretation of the kinetic complexity is that the RCs are heterogeneous. The excitation flash could create two populations of excited RCs (I and II) with different spectroscopic characteristics and electron-transfer kinetics. Such heterogeneity has been suggested by Kirmaier and Holten (1990) to account for the wavelength dependence of kinetics measured near 800 nm. However, if k_1 in Scheme III is set equal to 0 and the relative initial amounts of states I and II are varied, the result is calculated spectra for these states that have little resemblance to each other (not shown). One of the calculated spectra always includes positive features in the 940-nm region that seem physically implausible for the spectrum of an excited state of P.

Several recent reports have described multiexponential kinetics of spontaneous fluorescence from wild-type RCs at room temperature (Du et al., 1992; Hamm et al., 1993). Vos et al. (1991, 1992) have also described a biexponential decay of stimulated emission at 100 K. In our experiments, the kinetics measured with wild-type RCs was exponential even at low temperatures. Although there are several possible explanations for these variations in experimental results, the previous studies differed from ours in their use of much shorter excitation pulses. An ultrashort pulse can coherently excite multiple vibrational modes that fall within its relatively large spectral width. As the wave-packet evolves on the excited-state electronic surface, the absorption and emission spectra of the molecule can show oscillatory behavior. Overdamped oscillations superimposed on an exponentially decaying signal could have the appearance of a nonexponential decay. Such oscillations would not be observed if the excitation and probe pulses are longer than the relevant vibrational periods (Fragnito et al., 1989).

Electron-Transfer Kinetics. The effects of mutations of Tyr (M)210 on the initial charge-separation kinetics have been the subject of several previous studies (Nagarajan et al., 1990; Finkele et al., 1990). Chan et al. (1991a) observed a similar slowing of the initial electron-transfer reaction in *Rb. capsulatus* when the homologous Tyr (M)208 was replaced by phenylalanine. They found that the rate of the reaction was restored when the corresponding residue on the inactive branch, Phe (L)181, was simultaneously replaced by Tyr. When the residues at both sites were Tyr, Chan et al. observed an increase of ~75% in the electron-transfer rate compared to wild-type RCs. The symmetric influence of the substitution on the rate suggested that a polar residue in either position could serve to stabilize P^+.

Our results indicate that, although mutations of Tyr (M)-210 do indeed affect the stabilization of P^+ relative to P, the electrostatic stabilization of H_L^- is probably affected also. Whereas the destabilization of P^+ amounts to 33 ± 3 meV in the Ile mutant and to 30 ± 6 and 52 ± 10 meV in the Phe and Trp strains, respectively, the standard free energy of the relaxed $P^+H_L^-$ is increased by about 32 meV in the Ile mutant and by 46 and 69 meV in the Phe and Trp mutants, respectively (Table II). The effect on $P^+H_L^-$ is thus similar to the effect on P^+ in the Ile mutant, but approximately 16 meV larger in the Phe and Trp mutants. Electrostatic calculations based on the crystal structure of *Rps. viridis* have suggested that Tyr (M)210 may also stabilize B_L^- (Parson et al., 1990a,b).

At high temperatures, the rate constant of a nonadiabatic, endothermic, or weakly exothermic electron-transfer reaction is expected to depend on $\Delta G°$ and temperature, according to the expression

$$k = \frac{2\pi}{\hbar}\frac{|V|^2}{\sqrt{4\pi\lambda k_B T}}\exp\left\{-\frac{(\Delta G° + \lambda)^2}{4\lambda k_B T}\right\} \qquad (6)$$

where λ is the reorganization energy and V is the electronic coupling matrix element (Marcus & Sutin, 1985). This expression provides a useful framework for discussing the changes in rate of the mutant RCs, if we assume that the mutations affect only the free energies of the reactant or product states, leaving the reorganization energies and coupling matrix elements unchanged. For strongly exothermic reactions ($\Delta G° < -\lambda$), nuclear tunneling into excited vibrational modes of the product state can make the rate less sensitive to both $\Delta G°$ and temperature (Warshel et al., 1989).

$P^* \rightarrow P^+H_L^-$. There is a qualitative correlation between the rate of electron transfer to H_L and the free energy change, $\Delta G°_{P^*\rightarrow P+H^-}$: the rates are smaller in the mutant RCs, where $|\Delta G°|$ is smaller (Figure 4). This would be expected if $\Delta G° \approx -\lambda$ in wild-type RCs, as is suggested by the activationless nature of the reaction. According to eq 6, any change in $\Delta G°$ would make the reaction both slower and thermally activated (Marcus & Sutin, 1985; Bixon & Jortner, 1989). The fact that the reaction is temperature-independent in the Phe mutant and thermally activated in the Ile mutant could indicate a transition between the activationless and activated domains (Nagarajan et al., 1990). However, the observation that the change in $\Delta G°_{P^*\rightarrow P+H^-}$ is larger in the Phe mutant than in the Ile mutant (Table II), while at the same time the reaction is faster (Table I), complicates any description of the reaction in terms of a simple two-state problem. Additionally, the measured changes in $\Delta G°_{P^*\rightarrow P+H^-}$ appear to be too small to quantitatively account for the temperature dependence of the reaction in the Ile and Trp mutants. This is because when $\Delta G° \approx -\lambda$ the rate should be insensitive to small changes in $\Delta G°$. If we take $\Delta G°$ for wild-type RCs to be between −120 and −200 meV (Williams et al., 1992a; Table II), the change in $\Delta G°$ in the Ile mutant (32 meV, Table II) would give an activation energy [$E_a = (\Delta G° + \lambda)^2/4\lambda$] of only 1–2 meV, whereas the apparent activation energy of the electron-transfer reaction in this mutant is about 50 meV (Nagarajan et al., 1990).

A plausible resolution of these problems can be found by considering the role of $P^+B_L^-$. As mentioned above, two possible roles for this state have been suggested. The initial electron-transfer reaction could proceed through $P^+B_L^-$ as a distinct kinetic intermediate or proceed in a single step that requires superexchange with $P^+B_L^-$ as a virtual intermediate. These possibilities are not mutually exclusive. If $P^+B_L^-$ lies sufficiently close to P* in energy, both mechanisms would be expected to operate in parallel, as shown in Scheme IV. Bixon et al. (1991) have investigated this model in detail and have discussed how the overall electron-transfer rate would depend on the standard free energy gap between P* and $P^+B_L^-$ ($\Delta G°_{P^*\rightarrow P+B^-}$) and on temperature. They also considered the consequences of replacing Tyr (M)210 with Phe, which had been estimated to increase the free energy of $P^+B_L^-$ by approximately 1000 cm^{-1} (Parson et al., 1990a). Bixon et al. determined a range of values of $\Delta G°_{P^*\rightarrow P+B^-}$, for which the electron-transfer rate in the mutant RCs would be both slower than in the wild-type and thermally activated, in accord with the experimental findings. Here, we will incorporate the observation that the mutations also affect the free energy of $P^+H_L^-$.

Scheme IV

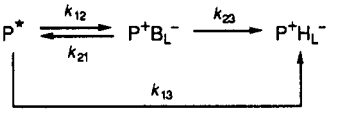

Using eq 6, the time constant τ for the decay of P* can be expressed in terms of the free energy gaps, reorganization energies, and coupling matrix elements for the individual steps in Scheme IV. To this end, it is useful to model the steps P* → $P^+B_L^-$ and P* → $P^+H_L^-$ with parabolic free energy functions of independent reaction coordinates, as shown in Figure 7. The angle θ between the coordinates for the two reactions can be used to parametrize the degree of coupling between the two reorganization processes. The reorganization energy for the second step in the two-step route ($P^+B_L^-$ → $P^+H_L^-$) and the coupling matrix element for the superexchange process then can be expressed in terms of θ and the reorganization energies and $\Delta G°$'s of the other steps (Appendix I). Since the

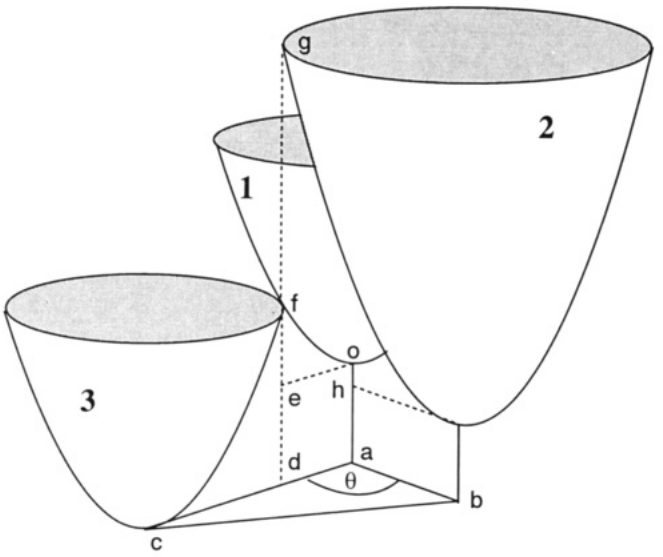

FIGURE 7: Schematic representation of the reaction coordinates for electron transfer. Parabolic free energy surfaces 1, 2, and 3 represent P*, $P^+B_L^-$, and $P^+H_L^-$, respectively. Lines ab and ac, the reaction coordinates for P* → $P^+B_L^-$ and P* → $P^+H_L^-$, are separated by angle θ. The displacements ab, ac, and bc are $(2\lambda_{1\rightarrow2}/\kappa)^{1/2}$, $(2\lambda_{1\rightarrow3}/\kappa)^{1/2}$, and $(2\lambda_{2\rightarrow3}/\kappa)^{1/2}$, where κ is the curvature of the surfaces; κ is taken to be the same for both coordinates. The activation energy for P* → $P^+H_L^-$ (E_a) is ef, and ad = $(2ef)/\kappa)^{1/2}$; fg is the free energy difference between surfaces 2 and 3 at the intersection of 1 and 3 (δE). The free energy changes $\Delta G^\circ_{P^*\rightarrow P+B^-}$ and $\Delta G^\circ_{P^*\rightarrow P+H^-}$ are oh and oa.

two charge-separation processes P* → $P^+B_L^-$ and P* → $P^+H_L^-$ both involve oxidation of P, their reaction coordinates would be expected to have a parallel component, so that values of θ in the range $0° < \theta < 90°$ seem physically plausible.

A lower limit for $\Delta G^\circ_{P^*\rightarrow P+B^-}$ in wild-type RCs can be obtained from the studies of Kirmaier et al. (1991) on the mutant (M)L214H. RCs of this mutant contain a bacteriochlorophyll in place of bacteriopheophytin H_L. Kirmaier et al. found that $\Delta G^\circ_{P^*\rightarrow P+H^-}$ was reduced in amplitude to about −75 mV. Although the electron-transfer time constant lengthened to ~6.4 ps at room temperature and 2.5 ps at 5 K, there was no indication of transient accumulation of $P^+B_L^-$. On the basis of this observation, Kirmaier et al. (1991) concluded that $\Delta G^\circ_{P^*\rightarrow P+B^-} > -75$ meV (−600 cm^{-1}).

After fixing $\Delta G^\circ_{P^*\rightarrow P+H^-}$ at its experimentally determined value (ca. −1200 cm^{-1}), we varied $\Delta G^\circ_{P^*\rightarrow P+B^-}$ with the constraint $\Delta G^\circ_{P^*\rightarrow P+B^-} > -600$ cm^{-1} and sought combinations of values for this parameter and the reorganization energies and coupling matrix elements that reproduced the experimentally observed electron-transfer rate and its temperature dependence for wild-type RCs. This was done with various values of θ between 0 and 90°. A parameter set that qualitatively reproduces the kinetics in wild-type RCs is as follows: $\Delta G^\circ_{P^*\rightarrow P+B^-} = -500$ cm^{-1}, $\lambda_{P^*\rightarrow P^+B^-} = 700$ cm^{-1}, $\lambda_{P^*\rightarrow P^+H^-} = 1500$ cm^{-1}, $V_{P^*\leftrightarrow P^+B^-} = 13$ cm^{-1} and $V_{P^+B^-\leftrightarrow P^+H^-} = 25$ cm^{-1}. The coupling matrix elements are similar to the estimates that have been calculated by semiempirical molecular orbital treatments on the basis of the *Rp. viridis* crystal structure (Parson & Warshel, 1987; Plato et al., 1988; Scherer & Fischer, 1989). Figure 8 shows the calculated temperature dependence of the rate for three values of θ: 20°, 30°, and 40°. The fraction of the reaction proceeding through the two-step channel is about 0.3 with θ = 20° and 0.6 with θ = 40°.

Since the change in $\Delta G^\circ_{P^*\rightarrow P+H^-}$ is measured experimentally, the only free parameter for the mutant RCs is the change in $\Delta G^\circ_{P^*\rightarrow P+B^-}$. By adjusting this parameter, one can reproduce the temperature dependence qualitatively for each mutant strain and get the room-temperature time constant to within a factor of 2 of the experimental value (Figure 8). The absolute time constant at room temperature primarily depends on $\Delta G^\circ_{P^*\rightarrow P+H^-}$ alone, whereas the two free energies together determine the temperature dependence. In all cases, the first term on the right in eq A1 of the Appendix was found to be negligible, so that the predicted kinetics was essentially monoexponential. For θ = 40°, the calculated maximum transient concentration of $P^+B_L^-$ varied between 1 and 15% of the initial concentration of P*, depending on the temperature and the ΔG° values. Kirmaier and Holten (1991), on the basis of measurements at 695 nm where B_L^- is expected to absorb, have placed an upper limit of 0.6 ps on the lifetime of $P^+B_L^-$ which, together with the 3-ps decay time for the stimulated emission, leads to an upper limit of ~12% for the transient $P^+B_L^-$ concentration in wild-type RCs. Our analysis seems consistent with this limit. As stated in the Results, small absorbance changes associated with the formation of $P^+B_L^-$ could be buried in the sub-picosecond kinetic component that we observed at room temperature.

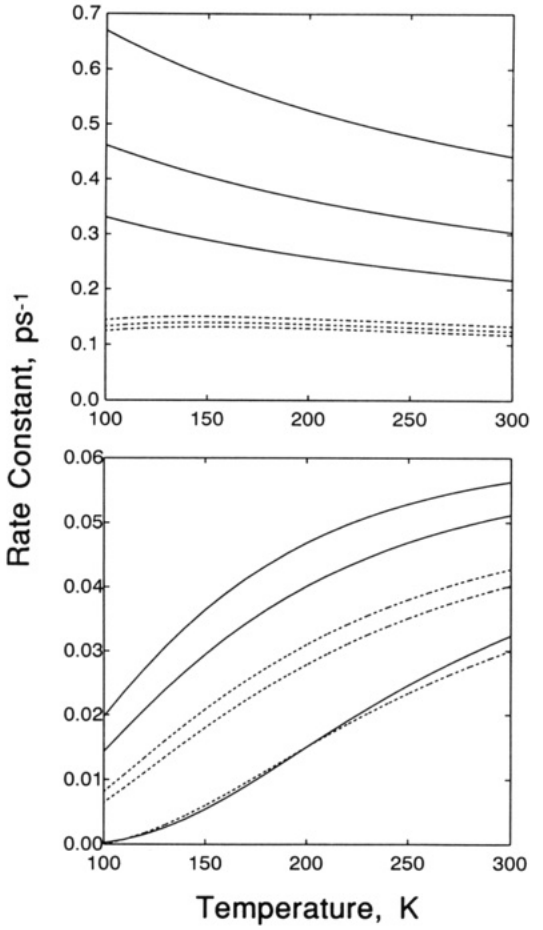

FIGURE 8: Calculated rate constants for the reaction P* → $P^+H_L^-$ as a function of temperature and θ for various values of $\Delta\Delta G^\circ_{P^*\rightarrow P+H^-}$ and $\Delta\Delta G^\circ_{P^*\rightarrow P+B^-}$. The curves were generated as described in the text and Appendix I, using the following parameters for wild-type RCs: $\Delta G^\circ_{P^*\rightarrow P+B^-} = -500$ cm^{-1}; $\Delta G^\circ_{P^*\rightarrow P+H^-} = -1200$ cm^{-1}; $\lambda_{P^*\rightarrow P^+B^-} = 700$ cm^{-1}; $\lambda_{P^*\rightarrow P^+H^-} = 1500$ cm^{-1}; $V_{P^*\leftrightarrow P^+B^-} = 13$ cm^{-1}; and $V_{P^+B^-\leftrightarrow P^+H^-} = 25$ cm^{-1}. In the top panel, the three solid lines were obtained with $\Delta\Delta G^\circ_{P^*\rightarrow P+H^-} = \Delta\Delta G^\circ_{P^*\rightarrow P+B^-} = 0$, and the broken lines with $\Delta\Delta G^\circ_{P^*\rightarrow P+H^-} = \Delta\Delta G^\circ_{P^*\rightarrow P+B^-} = 200$ cm^{-1}. In both sets of curves, θ = 20°, 30°, and 40° for the upper, middle, and lower curves, respectively. In the bottom panel, the solid lines were obtained with $\Delta\Delta G^\circ_{P^*\rightarrow P+B^-} = 500$ cm^{-1} and $\Delta\Delta G^\circ_{P^*\rightarrow P+B^-} = 150$ cm^{-1} and the broken lines with $\Delta\Delta G^\circ_{P^*\rightarrow P+B^-} = 600$ cm^{-1} and $\Delta\Delta G^\circ_{P^*\rightarrow P+H^-} = 350$ cm^{-1}. In both of these sets, θ = 20°, 30°, and 40° for the lower, middle, and upper curves, respectively.

For all of the mutants, it was necessary to use non-zero values for $\Delta\Delta G^{\circ}_{P^*\rightarrow P^+B^-}$ in order to reproduce the experimental results even approximately. The necessary magnitude of $\Delta\Delta G^{\circ}_{P^*\rightarrow P^+B^-}$ depended on the value of θ, but for $\theta > 0°$ it was always $\gtrsim\Delta\Delta G^{\circ}_{P^*\rightarrow P^+H^-}$. Also, in the parameter space explored, the necessary increases in the free energy of $P^+B_L^-$ were consistently larger than the increases that would have been obtained by considering only the changes in the E_m of P/P^+ (see Figure 8 and Table II). This is consistent with the idea that the mutations, in addition to influencing the E_m of P, also destabilize B_L^- and that their effects on $P^+B_L^-$ are, if anything, greater than the effects on $P^+H_L^-$. As noted earlier, the lack of a close correlation between the experimentally measured E_m of P and the free energy of $P^+H_L^-$ suggests an influence of the residue at (M)210 on the stabilization of H_L^-.

The electron-transfer rate and temperature dependence in the (M)L214H mutant (Kirmaier et al., 1991) could be well fit with the parameter set used for wild-type RCs by adjusting only the free energy of $P^+H_L^-$ to match the experimentally measured value for that strain (data not shown). No shift in the free energy of $P^+B_L^-$ was needed in this case. This is in accord with the expectation that the free energy of $P^+B_L^-$ would be relatively insensitive to mutations at a site removed from both P and B_L.

We conclude that the decrease in the primary electron-transfer rate and the increasing dependence of the rate on temperature as we go from Tyr to Phe, Ile, or Trp at (M)210 can be reasonably ascribed to an increased destabilization of $P^+B_L^-$ in the order mentioned. Although the increases in the free energies of $P^+B_L^-$ and $P^+H_L^-$ in the mutant RCs are attributable largely to the destabilization of P^+, to account for the temperature dependence of the kinetics it also appears necessary to postulate a significant destabilization of B_L^-. Such an effect had been predicted for the Phe mutant by electrostatics calculations (Parson et al., 1990a,b). The greater increases in the free energies in the Ile and Trp mutants were not anticipated and have not yet been explored by electrostatics calculations.

This phenomenological analysis of the electron-transfer kinetics rests on the possibly simplistic assumption that the electronic coupling matrix element, the free energy gap, and the reorganization energy are all relatively independent of temperature. We also have assumed that only the free energies are affected greatly in the mutants. It is possible that the apparent activationless kinetics in wild-type RCs results from a strengthening of the electronic coupling as the protein contracts with decreasing temperature (Kirmaier & Holten, 1988; Lous & Hoff, 1989). Fluorescence measurements have suggested that the free energy gap is temperature-dependent (Woodbury & Parson, 1984), and the reorganization energy could be as well. Molecular dynamics simulations (Parson et al., 1990b) have indicated that the reorganization energy for the formation of $P^+B_L^-$ may be decreased in the Tyr mutant. However, a decrease in the reorganization energy of $P^+H_L^-$ would not, in itself, account for the enhanced temperature sensitivity of the initial electron-transfer kinetics in the mutants.

$P^+Q_A^- \rightarrow PQ_A$. The rate of the $P^+Q_A^-$ recombination reaction increases with decreasing temperature (Figure 5). Since Tyr (M)210 is relatively far from the quinone, mutations at this site would be expected to change the free energy difference between $P^+Q_A^-$ and PQ_A approximately in proportion to their effect on the E_m of P. However, the observed changes in the electron-transfer rates at room temperature bear no simple relationship to the calculated $\Delta\Delta G°$ values (Figure 7). The 2-fold increase in rate in the Trp mutant is particularly difficult to explain on the basis of eq 6. If $\Delta G° > -\lambda$, the reaction would be expected to speed up when $\Delta G°$ becomes more negative. However, since $\Delta G° \approx -0.52$ eV (Arata & Parson, 1981), λ would have to be very large ($\sim$1 eV) in order for the rate to double in response to the estimated change in $\Delta G°$ (0.05 eV, Table II). This large difference between $\Delta G°$ and λ is difficult to reconcile with the temperature dependence of the reaction (Figure 5). Williams and co-workers (Williams et al., 1992b; J. C. Williams, personal communication) have observed a less pronounced dependence of the room-temperature recombination rate on $\Delta G°$ in a series of mutants with modified hydrogen bonding to the carbonyl groups of the dimer bacteriochlorophylls.

Because P is about 30 Å from Q_A, the direct electronic coupling between them is undoubtedly very small, and a higher order coupling through one or more intermediates is likely. Franzen et al. (1990) and Franzen and Boxer (1993), who analyzed the dependence of the reaction rate on $\Delta G°$ as modulated by an external electric field, have invoked superexchange coupling through $P^+H_L^-$. Although we could expand our model to include this coupling, the proliferation of variables would limit the utility of this exercise. Instead, it seems best to note that mutations sometimes result in unanticipated structural changes that cannot be assessed critically in the absence of crystallographic information.

ACKNOWLEDGMENT

We thank Werner Mäntele for much helpful advice on the construction of the electrochemical cell and Christine Suver for performing some of the electrochemical titrations.

APPENDIX I

In Scheme IV, the time-dependent concentration of P* is (Bixon et al., 1991)

$$[P^*] = \frac{s_- + k_{21} + k_{23}}{\delta} e^{s-t} - \frac{s_+ + k_{21} + k_{23}}{\delta} e^{s+t} \quad (A1)$$

with

$$\delta = \sqrt{(k_{13} + k_{12} + k_{21} + k_{23})^2 - 4(k_{13}k_{21} + k_{13}k_{23} + k_{12}k_{23})}$$

$$s_+ = -(k_{13} + k_{12} + k_{21} + k_{23} + \delta)/2 \quad \text{and}$$

$$s_- = -(k_{13} + k_{12} + k_{21} + k_{23} - \delta)/2$$

The experimentally measured time constant, τ, for the decay of P* can be equated to the integral of [P*] from $t = 0$ to ∞:

$$\tau = \int_0^\infty [P^*]\, dt = \frac{k_{21} + k_{23}}{s_+ s_-} \quad (A2)$$

To express the microscopic rate constants k_{ij} in terms of the free energy gaps, reorganization energies, and coupling matrix elements, we used eq 6 and

$$k_{21} = k_{12} \exp(\Delta G_{P^*\rightarrow P^+B^-}/k_B T) \quad (A3)$$

The coupling matrix element for the superexchange step is given by

$$V_{13} = V_{12}\{(1 - \delta E(\delta E^2 + 4V_{23}^2)^{-1/2})/2\}^{1/2} + V_{23}\{(1 - \delta E(\delta E^2 + 4V_{12}^2)^{-1/2})/2\}^{1/2} \quad (A4)$$

where δE is the energy separation between states $P^+B_L^-$ and $P^+H_L^-$, measured at the intersection of the free energy surfaces of P* and $P^+H_L^-$. (Equation A4 reduces to $V_{13} = 2V_{12}V_{23}/\delta E$ when $\delta E \gg V_{23}$, but this approximation was not applicable

in most of the situations considered here.) The energy difference δE can be equated to the free energy difference indicated in Figure 7, if the curvatures of the free energy surfaces are the same for all three states. If the angle θ between the reaction coordinates for $P^* \rightarrow P^+B_L^-$ and $P^* \rightarrow P^+H_L^-$ is defined as in Figure 7, the following relationships can easily be derived: where E_a is the activation energy for $P^* \rightarrow P^+H_L^-$.

$$\lambda_{2\rightarrow 3} = |(\lambda_{1\rightarrow 2} + \lambda_{1\rightarrow 3} + 2(\lambda_{1\rightarrow 2}\lambda_{1\rightarrow 3})^{1/2} \cos\theta| \quad \text{(A5)}$$

$$\delta E = |\Delta G^{\circ}_{P^*\rightarrow P+B^-} + \lambda_{1\rightarrow 2} - 2(\lambda_{1\rightarrow 2}E_a)^{1/2} \cos\theta|$$

REFERENCES

Allen, J. P., Feher, G., Yeates, T. O., Komiya, H., & Rees, D. C. (1987) *Proc. Natl. Acad. Sci. U.S.A. 84*, 5730–5734.

Arata, H., & Parson, W. W. (1981) *Biochim. Biophys. Acta 638*, 201–209.

Becker, M., Nagarajan, V., & Parson, W. W. (1991) *J. Am. Chem. Soc. 113*, 6840–6848.

Bixon, M., & Jortner, J. (1989) *Chem. Phys. Lett. 159*, 17–20.

Bixon, M., Jortner, J., & Michel-Beyerle, M. E. (1991) *Biochim. Biophys. Acta 1056*, 301–315.

Blankenship, R. E., & Parson, W. W. (1979) *Biochim. Biophys. Acta 545*, 429–444.

Boxer, S. G., Chidsey, C. E. D., & Roelofs, M. G. (1983) *Annu. Rev. Phys. Chem. 34*, 389–417.

Breton, J., Martin, J.-L., Petrich, J., Migus, A., & Antonetti, A. (1986) *FEBS Lett. 209*, 37–43.

Chan, C.-K., Chen, L. X.-Q., DiMagno, T. J., Hanson, D. K., Nance, S. L., Schiffer, M., Norris, J. R., & Fleming, G. R. (1991a) *Chem. Phys. Lett. 176*, 366–372.

Chan, C.-K., DiMagno, T. J., Chen, L. X.-Q., Norris, J. R., & Fleming, G. R. (1991b) *Proc. Natl. Acad. Sci. U.S.A. 88*, 11202–11206.

Chang, D.-H., Tiede, D., Tang, J., Smith, U., Norris, J., & Schiffer, M. (1986) *FEBS Lett. 205*, 82–86.

Chu, Z.-T., Warshel, A., & Parson, W. W. (1989) *Photosynth. Res. 22*, 39–46.

Deisenhofer, J., & Michel, H. (1989) *Science 245*, 1463–1473.

Du, M., Rosenthal, S., Xie, X., DiMagno, T. J., Schmidt, M., Hanson, D. K., Schiffer, M., Norris, J. R., & Fleming, G. R. (1992) *Proc. Natl. Acad. Sci. U.S.A. 89*, 8517–8521.

Finkele, U., Lauterwasser, C., Zinth, W., Gray, K., & Oesterhelt, D. (1990) *Biochemistry 29*, 8517–8521.

Fleming, G. R., Martin, J.-L., & Breton, J. (1988) *Nature 333*, 190–192.

Fragnito, H. L., Bigot, J.-Y., Becker, P. C., & Shank, C. V. (1989) *Chem. Phys. Lett. 160*, 101–104.

Franzen, S., & Boxer, S. G. (1993) *J. Phys. Chem. 97*, 6304–6318.

Franzen, S., Goldstein, R. F., & Boxer, S. G. (1990) *J. Phys. Chem. 94*, 5135–5149.

Goldstein, R. A., & Boxer, S. (1989) *Biochim. Biophys. Acta 977*, 70–77.

Gunner, M. R., & Dutton, P. L. (1989) *J. Am. Chem. Soc. 111*, 3400–3412.

Gunner, M. R., Robertson, D. E., & Dutton, P. L. (1986) *J. Phys. Chem. 90*, 3783–3795.

Hamm, P., Gray, K. A., Oesterhelt, D., Feick, R., Scheer, H., & Zinth, W. (1993) *Biochim. Biophys. Acta 1142*, 99–105.

Hofrichter, J., Henry, E. R., Sommer, J. H., Deutsch, R., Ikedo-Saito, M., Yonetani, T., & Eaton, W. A. (1985) *Biochemistry 24*, 2667–2679.

Holzapfel, W., Finkele, U., Kaiser, W., Oesterhelt, D., Scheer, H., Stilz, H. U., & Zinth, W. (1990) *Proc. Natl. Acad. Sci. U.S.A. 87*, 5168–5172.

Kirmaier, C., & Holten, D. (1988) in *The Photosynthetic Bacterial Reaction Center* (Breton, J., & Verméglio, A., Eds.) pp 219–228, Plenum Press, New York.

Kirmaier, C., & Holten, D. (1990) *Proc. Natl. Acad. Sci. U.S.A. 87*, 3552–3556.

Kirmaier, C., & Holten, D. (1991) *Biochemistry 30*, 609–613.

Kirmaier, C., Holten, D., & Parson, W. W. (1985) *Biochim. Biophys. Acta 810*, 33–48.

Kirmaier, C., Gaul, D., DeBey, R., Holten, D., & Schenck, C. C. (1991) *Science 251*, 922–927.

Kleinfeld, D., Okamura, M. Y., & Feher, G. (1984) *Biochemistry 23*, 5780–5786.

Lous, E. J., & Hoff, A. J. (1989) *Biochim. Biophys. Acta 974*, 88–103.

Marcus, R. A., & Sutin. N. (1985) *Biochim. Biophys. Acta 811*, 265–322.

McKubre, M. C. H., & Macdonald, D. D. (1984) in *Comprehensive Treatise of Electrochemistry; Volume 8—Experimental Methods in Electrochemistry* (White, R. E., Bockris, J. O'M., Conway, B. E., & Yeager, E., Eds.) pp 1–98, Plenum Press, New York.

Moss, D., Nabedryk, E., Breton, J., & Mäntele, W. (1990) *Eur. J. Biochem. 187*, 565–572.

Moss, D. A., Leonhard, M., Bauscher, M., & Mäntele, W. (1991) *FEBS Lett. 283*, 33–36.

Mourou, G. A., & Sizer, T. L., II (1982) *Opt. Commun. 41*, 47–48.

Nagarajan, V., Parson, W. W., Gaul, D., & Schenck, C. (1990) *Proc. Natl. Acad. Sci. U.S.A. 87*, 7888–7892.

Ogrodnik, A., Krüger, H. W., Orthuber, H., Haberkorn, R., Michel-Beyerle, M. E., & Scheer, H. (1982) *Biophys. J. 39*, 91–95.

Parson, W. W., & Warshel, A. (1987) *J. Am. Chem. Soc. 109*, 6152–6163.

Parson, W. W., Chu, Z.-T., & Warshel, A. (1990a) *Biochim. Biophys. Acta 1017*, 251–272.

Parson, W. W., Nagarajan, V., Gaul, D., Schenck, C. C., Chu, Z.-T., & Warshel, A. (1990b) in *Reaction Centers of Photosynthetic Bacteria* (Michel-Beyerle, M. E., Ed.) pp 239–250, Springer-Verlag, New York.

Plato, M., Möbius, K., Michel-Beyerle, M. E., Bixon, M., & Jortner, J. (1988) *J. Am. Chem. Soc.. 110*, 7279–7285.

Press, W. H., Flannery, B. P., Teukolsky, S. A., & Vetterling, W. T. (1989) *Numerical Recipes*, Cambridge University Press, New York.

Schenck, C. C., Blankenship, R. E., & Parson, W. W. (1982) *Biochim. Biophys. Acta 680*, 44–59.

Scherer, P. O. J., & Fischer, S. F. (1989) *Chem. Phys. 131*, 115–127.

Schilt, A. A. (1960) *J. Am. Chem. Soc. 82*, 3000–3005.

Schilt, A. A., & Cresswell, A. M. (1966) *Talanta 13*, 911–918.

Taniguchi, I., Toyosawa, K., Yamaguchi, H., & Yasukuochi, K. (1982) *J. Electroanal. Chem. 140*, 187–193.

Vos, M. H., Lambry, J.-C., Robles, S. J., Youvan, D. C., Breton, J., & Martin, J.-L. (1991) *Proc. Natl. Acad. Sci. U.S.A. 88*, 8885–8889.

Vos, M. H., Lambry, J.-C., Robles, S. J., Youvan, D. C., Breton, J., & Martin, J.-L. (1992) *Proc. Natl. Acad. Sci. U.S.A. 89*, 613–617.

Vos, M. H., Rappaport, F., Lambry, J.-C., Breton, J., & Martin, J.-L. (1993) *Nature 363*, 320–325.

Warshel, A., Chu, Z. T., & Parson, W. W. (1989) *Science 246*, 112–116.

Williams, J. C., Alden, R. G., Murchison, H. A., Peloquin, J. M., Woodbury, N. W., & Allen, J. P. (1992a) *Biochemistry 31*, 11029–11037.

Williams, J. C., Woodbury, N. W., Taguchi, A. K. W., Peloquin, J. M., Alden, R. G., & Allen, J. P. (1992b) in *The Photosynthetic Bacterial Reaction Center II: Structure, Spectroscopy and Dynamics*, (Breton, J., & Verméglio, A., Eds.) pp 25–31, Plenum Press, New York.

Woodbury, N. W. T., & Parson, W. W. (1984) *Biochim. Biophys. Acta 767*, 345–361.

Woodbury, N. W. T., Becker, M., Middendorf, D., & Parson, W. W. (1985) *Biochemistry 24*, 7516–7521.

Zankel, K. L., Reed, D. W., & Clayton, R. K. (1968) *Proc. Natl. Acad. Sci. U.S.A. 61*, 1243–1249.